

REPORT DOCUMENTATION PAGE			Form Approved OMB NO. 0704-0188		
<p>The public reporting burden for this collection of information is estimated to average 1 hour per response, including the time for reviewing instructions, searching existing data sources, gathering and maintaining the data needed, and completing and reviewing the collection of information. Send comments regarding this burden estimate or any other aspect of this collection of information, including suggestions for reducing this burden, to Washington Headquarters Services, Directorate for Information Operations and Reports, 1215 Jefferson Davis Highway, Suite 1204, Arlington VA, 22202-4302. Respondents should be aware that notwithstanding any other provision of law, no person shall be subject to any penalty for failing to comply with a collection of information if it does not display a currently valid OMB control number. PLEASE DO NOT RETURN YOUR FORM TO THE ABOVE ADDRESS.</p>					
1. REPORT DATE (DD-MM-YYYY) 19-11-2018		2. REPORT TYPE Final Report		3. DATES COVERED (From - To) 15-Sep-2014 - 14-Mar-2017	
4. TITLE AND SUBTITLE Final Report: Novel Epitaxial Films of Magnetolectric Hexaferrite Materials			5a. CONTRACT NUMBER W911NF-14-1-0630		
			5b. GRANT NUMBER		
			5c. PROGRAM ELEMENT NUMBER 611102		
6. AUTHORS			5d. PROJECT NUMBER		
			5e. TASK NUMBER		
			5f. WORK UNIT NUMBER		
7. PERFORMING ORGANIZATION NAMES AND ADDRESSES Northeastern University 360 Huntington Avenue 490 RP Boston, MA 02115 -5005			8. PERFORMING ORGANIZATION REPORT NUMBER		
9. SPONSORING/MONITORING AGENCY NAME(S) AND ADDRESS (ES) U.S. Army Research Office P.O. Box 12211 Research Triangle Park, NC 27709-2211			10. SPONSOR/MONITOR'S ACRONYM(S) ARO		
			11. SPONSOR/MONITOR'S REPORT NUMBER(S) 62325-MS.3		
12. DISTRIBUTION AVAILABILITY STATEMENT Approved for public release; distribution is unlimited.					
13. SUPPLEMENTARY NOTES The views, opinions and/or findings contained in this report are those of the author(s) and should not be construed as an official Department of the Army position, policy or decision, unless so designated by other documentation.					
14. ABSTRACT					
15. SUBJECT TERMS					
16. SECURITY CLASSIFICATION OF:			17. LIMITATION OF ABSTRACT UU	15. NUMBER OF PAGES	19a. NAME OF RESPONSIBLE PERSON Carmine Vittoria
a. REPORT UU	b. ABSTRACT UU	c. THIS PAGE UU			19b. TELEPHONE NUMBER 617-373-2061

RPPR Final Report
as of 20-Nov-2018

Agency Code:

Proposal Number: 62325MS

Agreement Number: W911NF-14-1-0630

INVESTIGATOR(S):

Name: Ph.D. Carmine Vittoria

Email: c.vittoria@neu.edu

Phone Number: 6173732061

Principal: Y

Organization: **Northeastern University**

Address: 360 Huntington Avenue, Boston, MA 021155005

Country: USA

DUNS Number: 001423631

EIN: 104167998

Report Date: 14-Jun-2017

Date Received: 19-Nov-2018

Final Report for Period Beginning 15-Sep-2014 and Ending 14-Mar-2017

Title: Novel Epitaxial Films of Magnetoelectric Hexaferrite Materials

Begin Performance Period: 15-Sep-2014

End Performance Period: 14-Mar-2017

Report Term: 0-Other

Submitted By: Ph.D. Carmine Vittoria

Email: c.vittoria@neu.edu

Phone: (617) 373-2061

Distribution Statement: 1-Approved for public release; distribution is unlimited.

STEM Degrees: 2

STEM Participants: 2

Major Goals: The magnetoelectric effect in M-type Ti-Co doped strontium hexaferrite has been studied using magnetometry, ferromagnetic resonance, and soft X-ray spectroscopies. A large increase in the magnetoelectric coupling is found when Co ions enter the trigonal bi-pyramidal site. The increase is explained in terms of unusual displacement of magnetic transition (TM) ions in the site. An off-center displacement of the cation induces a large local electric dipole and increase in the magnetostriction constant and thereby the magnetoelectric coupling.

Accomplishments: We deposited magnetoelectric ferrites operational at room temperature exhibiting high linear coupling for the first time. We developed a deposition technique whereby magnetic ions were deposited at the atomic scale. We call this technique the ATLAD technique, alternating target laser ablation deposition.

Training Opportunities: Nothing to Report

Results Dissemination: Nothing to Report

Honors and Awards: Nothing to Report

Protocol Activity Status:

Technology Transfer: Nothing to Report

PARTICIPANTS:

Participant Type: PD/PI

Participant: Carmine Vittoria

Person Months Worked: 1.00

Funding Support:

Project Contribution:

International Collaboration:

International Travel:

National Academy Member: N

Other Collaborators:

Participant Type: Co-Investigator

FINAL REPORT

Carmine Vittoria
Northeastern University

Boston, MA 02115

Abstract

The magnetoelectric effect in M-type Ti-Co doped strontium hexaferrite has been studied using a combination of magnetometry and element specific soft X-ray spectroscopies. A large increase ($> \times 30$) in the magnetoelectric coefficient is found for samples in which Co^{2+} enters the trigonal bipyramidal site. The 5-fold trigonal bipyramidal site has been shown to provide an unusual mechanism for electric polarization based on the displacement of magnetic transition metal (TM) ions. We show that for Co entering this site an off-center displacement of the cation can induce a large local electric dipole as well as providing increased magnetostriction enhancing the magnetoelectric effect.

1. INTRODUCTION

The ability to control magnetism by an applied electric field is the “holy grail” in creating ultra-low power, high density MRAM. In this respect magnetoelectric (ME) multiferroics are currently an intense topic of research, not only in understanding how the two symmetry breaking orders can exist in the same material (they usually require either empty or partially filled transition metal orbitals respectively), but how the two ferroic orders can be coupled. Most ferromagnets are metallic but for ferroelectric order the material must be insulating to avoid screening of the electric field by the mobile carriers. As such most of the multiferroics reported so far have tended to be antiferromagnetic and ferroelectric, and only below room temperature with weak coupling (α) between the order parameters. Among the few room temperature single-phase ME multiferroics reported, hexaferrites seem to show potential for device applications as they exhibit a low field ME effect at room temperature [1].

Hexaferrites, iron oxides with hexagonal structures, are arranged in different repeating sequences of basic building blocks called R, S and T layers, where the S layer is a spinel structure. M-type hexaferrites can be described as a sequence of $\text{RSR}^* \text{S}^*$ (the * indicates a 180 degree rotation around the c axis) layers whereas the Z-types have a $\text{RSTSR}^* \text{S}^* \text{T}^* \text{S}^*$ sequence [2]. The unit cell of the archetypal M-type hexaferrite $\text{BaFe}_{12}\text{O}_{19}$ is shown in Fig.1. Fe^{3+} cations occupy both octahedral (O_h) and tetrahedral (T_d) co-ordinated sites in the S block (Wyckoff positions $2a$ and $4f_1$) and octahedral sites ($12k$ and $4f_2$) in the R block. The Ba ion located at $2d$ strongly distorts the octahedral site located at the $2b$ positions giving rise to a bi-pyramidal 5 fold co-ordination which is believed to induce a large uniaxial magnetic anisotropy parallel to the c-axis [3].

However, replacement of Ba with Sr and ionic Co^{2+} and Ti^{4+} substitutions dramatically alters the magnetic properties [4]. The smaller ionic radius of Sr compared to Ba changes the superexchange bond angle in Fe-O-Fe sites ($2a$ and $2b$ sites) near the Sr substitution from 116 degrees with Ba to

123 degrees with Sr [5]. Co^{2+} and Ti^{4+} ionic substitutions for Fe^{3+} also have great ramifications in terms of exchange interactions between magnetic ions, and magnetic anisotropy. Ti substitutions decrease the exchange coupling between spins in the R and S blocks whilst the effect of Sr and Co substitutions appears to be cumulative in that the net effect is the magnetic anisotropy changes from uniaxial to an easy cone of magnetization tilted away from the c-axis. The result of these substitutions (Sr, Ti, and Co) is to stabilize a non-collinear longitudinal conical magnetic structure []. For ME multiferroics the spiral magnetic state is of high interest as magnetically induced ferroelectrics are typically found when a complex magnetic order (spiral) exists [6]. In addition, Co and Ti doping in $\text{SrFe}_{12}\text{O}_{19}$ has been shown to increase the resistivity up to $\approx 10^{10} \Omega\text{cm}$, which is high enough to support an electric field [7].

The ME effect at room temperature in cobalt substituted M-type, $\text{SrFe}_8\text{Ti}_2\text{Co}_2\text{O}_{19}$, was first reported in bulk [8] and, thereafter, in thin films [9]. The effect of cobalt substitution on the ME coupling strength, α , in $\text{Sr}^{2+}\text{Co}_x^{2+}\text{Ti}_{3-0.5x}^{4+}\text{Fe}_8^{3+}\text{O}_{19}^{2-}$ was also reported in [11]. It was observed that Co ionic substitutions have a significant effect on the measured room temperature ME coupling with $\alpha(x)$ showing tensorial behaviour depending on whether the electric field is applied parallel or perpendicular to the magnetisation, $M[\mathbf{X}]$. Co^{2+} substitutions in ferrite structures are also a well-known source of magnetoelastic coupling due to the large orbital moment of Co^{2+} compared to Fe^{3+} [12]. The linear ME coupling is directly proportional to the magnetoelastic coupling, or magnetostriction, λ , implying that an increase in λ increases α []. However, this picture is oversimplified in that the material also requires a mechanism, such as the piezoelectric effect or electrostriction, for coupling the applied electric field into strain. Several mechanisms for magnetically induced ferroelectricity have been proposed. Jia *et al* (16, 17) classify the origin of magnetically induced ferroelectric polarization into three main mechanisms: the exchange-striction mechanism, spin-current mechanism, and d-p hybridization mechanism. In the exchange-striction mechanism, ferroelectricity is attributed to crystallographic deformations induced by changing bonding as a result of a magnetic order. The spin current mechanism can be regarded as an inverse effect of the antisymmetric Dzyaloshinskii - Moriya (DM) interaction (24, 25) in which two non-collinearly coupled magnetic moments displace the exchange mediating ligand ion between them. This mechanism was first proposed by Katsura and co-workers (23) and predicts that if the magnetic moments are aligned in a cycloidal spiral manner the total electric polarization can be finite and in the direction perpendicular to both the spin spiral axis and the magnetic modulation vector \mathbf{Q} . This mechanism is typically found in the ME hexaferrites including the M-types. The final mechanism is due to the spin dependent p-d hybridization between the transition metal cation and the ligand anion which can induce a nonzero polarization for partially filled t_{2g} orbitals.

Recently a unique magnetic-ion-induced displacive electric polarization was reported in $(\text{Ba,Sr})\text{Fe}_{12}\text{O}_{19}$ [] providing a further route for multiferroicity in hexaferrites. The authors demonstrated that the competition between long range Coulomb interactions and short range Pauli repulsion in the $(\text{TM})\text{O}_5$ bipyramidal unit, unique to the hexaferrite structure, favours an off centre displacement of the TM ion inducing a local electric dipole. The role of the bipyramidal trigonal to magnetoelectric effects in these materials has not received significant attention as yet but it seems that it may be important in several of the mechanisms, i.e due to the displacement of the magnetoelastic ion resulting in a non-centrosymmetric nature local environment and its role in the non-collinearity of the spins in the structure.

In this article we show that the magnetoelectric coefficient, α , can be significantly enhanced by doping Co^{2+} into the R-block of the hexaferrite structure which contains the 5-fold bipyramidal trigonal site. The bipyramidal trigonal site allows for a large off centre displacement of the

magnetoelastic Co cation providing a local electric dipole, ideal properties for magnetoelectric materials.

2. EXPERIMENTAL DETAILS

The samples were grown by pulsed laser deposition (PLD) on single crystal sapphire (0001) substrates at 600°C under a 200±5 mtorr partial pressure of oxygen. The alternating target laser deposition technique (ATLAD) was used to deposit Co and Ti ions in the S or R block of the ME hexaferrite material, allowing for different site occupancies compared to deposition from a single target [13]. In the deposition the R block was simulated by depositing from a target of $\text{SrFe}_{(4-\delta)}\text{Ti}_{0.5\delta}\text{Co}_{0.5\delta}\text{O}_7$ and the S block was simulated by depositing from a target of $\text{Fe}_{(1+0.25\delta)}\text{Ti}_{0.5(1-0.25\delta)}\text{Co}_{0.5(1-0.25\delta)}\text{O}_3$. Three samples were grown with $\delta = 0.0, 0.2$ and 0.4 . It is noted that irrespective of the value of δ the chemical formula was held constant, $\text{SrFe}_8\text{Ti}_2\text{Co}_2\text{O}_{19}$, but for $\delta = 0$ the aim was to try and force Ti and Co ions to reside only in the S block. Deposited films were post-annealed in oxygen at 1050 °C for 40 minutes in order to increase the resistivity of the sample [1], and then capped with 2nm of Au.

XRD measurements were performed using a Rigaku SmartLab diffractometer with a Cu K-alpha source whilst magnetic measurements were performed using a Vibrating Sample Magnetometer (VSM-SQUID). For the ME coupling measurements a voltage, V, was applied across the film thickness and substrate with changes to the magnetization, as measured by VSM, recorded as a function of V. Ti $L_{2,3}$ XAS, Co $L_{2,3}$ and Fe $L_{2,3}$ XAS and XMCD measurements were performed on beamline I06 at the Diamond Light Source [14]. Total-electron yield (TEY) and fluorescence yield (FY) were monitored simultaneously using the sample drain current and the photocurrent of a diode mounted at 90° to the incident beam, respectively.

3. RESULTS

XRD patterns for the two films reveal the hexagonal P63/mmc structure with lattice spacings of $a = 5.87(2)$ Å, $c = 23.05(4)$ Å for $\delta = 0$, $a = 5.84(2)$ Å, $c = 23.05(4)$ Å for $\delta = 0.2$ and $a = 5.84(2)$ Å, $c = 23.05(4)$ Å for $\delta = 0.4$ which are in good agreement to the range of values found in the literature [2]. VSM magnetometry measurements were measured for the applied field parallel to the surface for temperatures between 5K and 450K. Fig.2(a,b,c) shows $M(T)$ measured in an applied field of 300 Oe after zero field cooling (ZFC) and field cooling (FC) at 30kOe. For the $\delta = 0.2$ field cooled case, Fig.2b, increasing the temperature from 10K causes the magnetization to steadily decrease as one would expect for a simple ferro / ferrimagnet material. However around 200K the slope of M vs T flattens before falling again. A similar effect is seen for $\delta = 0.4$ and for both samples the flattening of the slope in M vs T occurs at the same temperature as a peak seen in the ZFC data. This behaviour is not seen in $\delta = 0.0$, Fig.2a, which shows a shallower and nearly linear decrease in M over the same temperature range for the FC data. However a peak, albeit less pronounced, is also seen in the ZFC $M(T)$. The peak in the ZFC $M(T)$ data, seen in hexaferrites, is often interpreted as a change in magnetic order from a spin spiral to a collinear spin arrangement [] even though the microscopic origin of $M(T)$ is extremely complicated in multi-sublattice magnetic oxides. For a simple 2-sublattice system the discontinuities in $M(T)$ can be attributed to a number of effects such as a change between a collinear ferromagnetic order to an order with canted spins (spin spirals) or from a magnetic compensation point as has been discussed in detail by [3]. In systems with more than two

sublattices, such as the hexaferrites, it is not possible to infer the magnetic order directly from $M(T)$ without complementary information such as that provided by neutron diffraction []. However, in the M-type hexaferrites an easy cone of magnetization [15] develops when doping with Co-Ti above a critical level ($x = 1.1$) as a result of non-collinearity [] which also has the effect of dramatically reducing the coercivity. The angle of the cone was previously calculated to be 61 degrees from the c-axis at room temperature for a substitution level of $x = 1$.

Fig.2(c) show hysteresis loops for $\delta = 0, 0.2$ and 0.4 measured at 300K. With increasing temperature from 10K a sharp reduction in coercivity on crossing a critical temperature ($T_c = 170K$) for $\delta = 0.2$ is observed whilst a more gradual decrease for occurs for $\delta = 0.0$. At 300K the coercivity for $\delta = 0, 0.2$ and 0.4 is 720, 57 and xx Oe respectively compared to 2335, 1085 and yyy Oe at 10K. The large reduction in coercivity at 300K for $\delta = 0.2$ and 0.4 compared to $\delta = 0.0$ and non-Co-Ti doped SrM samples found in the literature [] is indicative of a large angle cone of magnetization as a result of non-collinearity.

The magnetoelectric effect is shown in Fig.x as the change in magnetisation, ΔM , as a function of applied electric voltage for (a) $\delta = 0$, (b) $\delta = 0.2$ and (c) $\delta = 0.4$. The measurements were taken in an applied magnetic field of 400 Oe.

The linear magneto-electric coefficient, α , is defined as [21]

$$\alpha = \mu_0 \frac{\partial M}{\partial E} \tag{Eq. (1)}$$

where $E = \frac{V}{d} \left(\frac{\epsilon_s}{\epsilon_f} \right)$ is the electric field across the film, V is the applied voltage across film and substrate, d is the thickness of the substrate and ϵ_s, ϵ_f are the relative permittivity's of the substrate and film respectively. The relative permittivity $\epsilon_s = 10$ for sapphire whilst for M-type hexaferrites $\epsilon_f \approx 5000$ [22] but is highly dependent on the conductivity of the film and therefore the amount of Fe^{2+} in the sample. Given we do not know the exact d.c value of ϵ_f for the films, but assume they are approximately equal for all three samples due to approximately amounts of Fe^{2+} , we calculate the ratio of the magnetoelectric coefficients for the two films to give

$$\Lambda_1 = \frac{\alpha(0.2)}{\alpha(0.0)} = 36$$

$$\Lambda_2 = \frac{\alpha(0.4)}{\alpha(0.0)} = 36$$

For $\delta = 0.2$, α has increased by over an order of magnitude compared to $\delta = 0.0$. Measurements on $\delta = 0.4$ also shows a large enhancement of α compared to the $\delta = 0.0$ film.

To gain a more detailed understanding of the role of Co-Ti substitutions in SrM, we performed XAS at the Ti $L_{2,3}$ absorption edge and XAS/XMCD measurements at the Co and Fe $L_{2,3}$ absorption edges in order to determine valency, co-ordination and the magnetic response of the individual elements. In L-edge XAS, electrons are excited from a 2p core level to the unoccupied 3d valence states of the element of interest by circularly polarized x rays at the resonance energies of the transitions. The

difference in absorption for opposite polarizations (the XMCD) gives a direct and element-specific measurement of the projection of the 3d magnetic moment along the x-ray polarization vector [16]. The absorption cross section is conventionally obtained by measuring the decay products, either fluorescent x-rays (FY) or electrons (TEY), of the photo-excited core hole. The type of decay product measured determines the probing depth of the technique. For transition metals at $L_{2,3}$ absorption, the probing depths for FY and TEY detection are 100 nm and 6 nm respectively.

Figure 4 shows the Ti XAS measured at the $L_{2,3}$ edges for $\delta = 0$. The spectra for $\delta = 0.2$ and 0.4 is nearly identical so only one is plotted. Four peaks are seen in the spectra. In octahedral symmetry, the crystal field splits the degenerate 3d orbitals into an e_g and a t_{2g} configuration where the t_{2g} consists of the d_{xy} , d_{xz} , and d_{yz} orbitals and the e_g configuration, the higher energy d_z^2 and $d_{x^2-y^2}$ orbitals. Thus two peaks are expected for each spin orbit split initial state ($2p^{3/2}$, $2p^{1/2}$). Excellent agreement between the experimental data and atomic multiplet calculations [17], shown as the solid line in Fig.3, is found for Ti^{4+} in an octahedral co-ordination with a crystal field parameter (10Dq) of 1.9eV. Fig.3 also shows the calculated spectra for Ti^{4+} in a tetrahedral co-ordination (dashed line). It is clear from the spectra that the Ti ions in both samples have a 4^+ valancy and occupy octahedral sites.

We now turn our attention to the magnetic Co and Fe cations. Figure 5 shows XAS and XMCD data for (a,d) $\delta = 0$, (b,e) $\delta = 0.2$ and (c,f) $\delta = 0.2$ at the Fe and Co $L_{2,3}$ edges respectively. The XAS at the Fe $L_{2,3}$ edges for all samples shows multiplet structure typical of an iron oxide. Three peaks (two negative and one positive) are present in the XMCD spectra, similar to that found for Fe_3O_4 [18].

The peaks correspond to contributions from Fe^{3+} in octahedral, Fe^{3+} in tetrahedral and Fe^{2+} in octahedral sites. For the M-type hexaferrite structure, spins located at the Fe tetrahedral sites are aligned anti-parallel to the majority of spins at the Fe octahedral sites [2]. Hence the positive peak in the XMCD is due to tetrahedrally co-ordinated Fe^{3+} . Fits to the XMCD data using atomic multiplet calculations show that XMCD spectra is best represented by $\sim 70\%$ octahedral co-ordinated and $\sim 30\%$ tetrahedral co-ordinated Fe. We note that this should not be taken as the relative Fe occupancy of the sites. For example the spins of octahedral co-ordinated Fe at the $4f_2$ sites are aligned anti-parallel to the other octahedral sites in the unit cell and therefore reduce the magnetic octahedral contribution to the XMCD signal. Interestingly the hexaferrite structure is usually considered to only contain Fe^{3+} . The occurrence of Fe^{2+} , probably due to incomplete oxidation during growth, is detrimental to magnetoelectric materials as it provides a conductive pathway, due to polaronic hopping, between the Fe^{2+} / Fe^{3+} ions located at octahedral sites, supressing electric polarisation. The XAS / XMCD data at the Co $L_{2,3}$ edges is shown in the bottom panel (c). The XAS lineshape is a superposition of Co^{2+} spectra in octahedral and tetrahedral environments. However the XMCD lineshape, which provides information on the uncompensated moments in the ferrimagnetic structure, is predominantly from Co^{2+} in an octahedral environment. Fits to the XMCD data using atomic multiplet calculations [19], show that the majority of the XMCD is due to octahedral Co ($\sim 70\%$) with a 30% tetrahedral contribution. As can be seen from the figure, the sign of the XMCD peak is negative, parallel to the majority of the Fe peaks indicating the net Co magnetic contribution is aligned parallel to the majority of the Fe spins. Thus for $\delta = 0$ the Co seems to have been substituted into both octahedral and tetrahedral sites whilst Ti has entered into only the octahedral sites. Which octahedral sites the Ti substitutes into cannot be determined from the XAS data. However, according to [20] Ti prefers the 12k positions and so for $\delta = 0$ the data is consistent with the aim to substitute Co-Ti into the S block only.

Fig.4b shows the Fe XAS and XMCD for $\delta = 0.2$. The XAS lineshape is similar to that for $\delta = 0$. However, atomic multiplet fits to the XMCD data reveal a smaller tetrahedral / octahedral ratio for

this sample compared to $\delta = 0$ (the amount of Fe^{2+} is the same for both $\delta = 0$ and 0.2 to within error). XAS and XMCD at the Co $L_{2,3}$ edges, Fig.4d, show differences in the XAS and XMCD lineshape compared to $\delta = 0$. A comparison of the XAS and XMCD data with an atomic multiplet calculation shows that the magnetic contribution from Co is mainly (~70%) from Co^{2+} ions in tetrahedral and trigonal sites. As can be seen from the Fig.4d the spins of the tetrahedral / trigonal co-ordinated Co^{2+} align anti-parallel with the octahedral Fe. Self-consistency is provided by a comparison between the Fe and Co data. The decreased tetrahedral / octahedral ratio for Fe is accompanied by an increase in the tetrahedral / octahedral ratio for Co.

4. DISCUSSION

We first discuss the Co XAS/XMCD data for the two films. For $\delta = 0.0$ the XAS lineshape can be modelled by a superposition of octahedral and tetrahedral Co^{2+} spectra. For $\delta = 0.0$ the Ti-Co substitution is intended to occur only in the S-block i.e. the 2a, $4f_1$ and 12k sites. It has been shown [2,8,20,23] that Ti has a strong preference for the 12k sites whilst Co^{2+} prefers the $4f_1$ and the 2a sites, although there is significant contradiction in the literature [8,20, 23]. The preference for Co^{2+} in the tetrahedral ($4f_1$) sites is reported to be due to the large Co^{2+} cation radius ($r_{\text{Co}(2+)} = 0.58 \text{ \AA}$) which stabilizes the S block compared to the smaller Fe^{3+} cation ($r_{\text{Fe}(3+)} = 0.49 \text{ \AA}$) [18]. However, Fe^{2+} , which has a larger ionic radius ($r_{\text{Fe}(2+)} = 0.63 \text{ \AA}$) than Co^{2+} , may modify this picture and force the Co^{2+} into the 2a or 12k sites. The XMCD spectrum clearly shows that the total magnetic contribution from the Co sites in the structure is parallel to the Fe octahedral sites and predominantly from Co^{2+} octahedrally co-ordinated.

For $\delta = 0.2$ the Co XAS spectra is a superposition of octahedral, trigonal and tetrahedral Co^{2+} spectra. As doping now takes place in the R and S block we consider that all sites can be occupied. A large change in the anisotropy, Fig.2, is seen for this sample which is likely to be due to substitution into the trigonal 2b site which is known to be responsible for the large anisotropy in the parent compound [2]. The magnetic contribution from the Co has a component anti-parallel to the Fe octahedral sites and a good fit to the XMCD spectra is based on a ~ 70:30 ratio of (tetrahedral + trigonal):octahedral. The Co moment, or at least a component of the moment, on the 2b trigonal site is anti-parallel to the majority of octahedral Fe cations which is in agreement with the finding of Williams *et al* for BaTiCoFeO [23].

For $\delta = 0.4$ the XAS and XMCD at the Co $L_{2,3}$ edges show an intriguing effect. Although the XAS spectra is dominated by Co^{2+} octahedrally co-ordinated, the XMCD shows the magnetic response is almost identical to that for $\delta = 0.2$ i.e. predominantly from tetrahedral and trigonal co-ordinated Co. We believe this can be explained by the fact that there must be a roughly equal amount of octahedral Co with opposite spins which contribute to the XAS but cancel each other out in the XMCD. However, the importance of Co^{2+} in the trigonal sites to the macroscopic magnetic properties such as the coercivity is clear. Further evidence of the importance of the bipyramidal trigonal to magnetoelectric effects in hexaferrites has recently been demonstrated by Shen *et al* [24] in which they show that the competition between long range Coulomb interactions and short range Pauli repulsion in a $(\text{TM})\text{O}_5$ bipyramidal unit favours an off centre displacement of the TM ion inducing a local electric dipole.

To provide further insight into the role of cation substitutions at the trigonal bipyramidal sites in the magnetoelectric coupling mechanisms, the M-type hexaferrite structure was simulated using materials studio [z]. Two structures were created, one that replicates strontium ferrite, $\text{SrFe}_{12}\text{O}_{19}$, in which Fe^{3+} ions occupy all interstitial lattice sites, and the other to replicate $\text{SrCo}_2\text{Ti}_2\text{Fe}_8\text{O}_{19}$ with the

Ti⁴⁺ ions occupying the 12K octahedral sites and the Co²⁺ ions at the trigonal bipyramidal sites. The geometries of the structures were optimised using the CASTEP 8.0 density functional theory, DFT, code [ZZZ]. The calculations were performed using the General Gradient Approximation, GGA, and the Perdew-Burke-Ernzerhof, PBE, functional. A cut off energy and convergence criteria of 1200eV and 10⁻⁶eV were used, respectively. The geometry optimisation for each structure was run until the residual force on each ion was less than 0.01eV/Å, with a total energy convergence tolerance of 5x10⁻⁶eV/atom, a geometry stress component tolerance of 0.02GPa and a maximum ionic displacement tolerance of 2x10⁻³Å. The calculations utilised the Broyden-Fletcher-Goldfarb-Shanno, BFGS, geometry method with the initial lattice constants for both the structures set to a = b = 5.88Å and c = 23.10Å. Having performed the geometry optimisation calculations the in plane and out of plane trigonal bipyramidal site bond lengths, r₀ and r₁, were extracted. Using the phenomenological local potential energy method for the bipyramid, as developed in [], the energy profile along the c-axis (z) was calculated using

$$U_{repulsion}(z) = 3\beta c_{+-} \exp\left[\left(r_+ + r_- - \sqrt{r_0^2 + z^2}\right)/\rho\right] + \beta c_{+-} \exp[(r_+ + r_- - (r_1 + z))/\rho] + \beta c_{+-} \exp[(r_+ + r_- - (r_1 - z))/\rho]$$

Eq. (2)

where r₀ and r₁ are the in-plane and out-of-plane TM-O distances in the bi-pyramid for 2b sites, β is a constant (taken to be 1.35 × 10⁻¹⁹ J), c₊₋ = 1 is Pauling's valence factor, and ρ = 0.314 Å [zzz]. r₊ = 1.4 (Å) are the ionic radii of Fe³⁺ and Co²⁺ with a co-ordinate number of 5 respectively and r₋ = 0.58 Å is the ionic radius of O²⁻ from ref [zzzzz].

The local potential energy profile along the c-axis for SrM where Fe³⁺ resides in all interstitial sites is shown in Fig.6a. Our data reproduces that reported in [], where the double well potential is indicative of an off centre displacement of the cation leading to a ferroelectric state. However, the energy barrier (ΔE) for SrM is only 2meV so that at room temperature the cation oscillates rapidly between the two minima resulting in an "average" equatorial position and no polarization. However on substitution of Co²⁺ into the 2b positions the situation changes. The differing r₀, r₁ and r₊ for Co compared to Fe increases the distance between the double well minima as well as the energy barrier between them. The separation of the minima increases from 0.3 Å for TM = Fe to 0.8 Å for TM = Co whilst the energy barrier increase from 2meV for TM = Fe to 100meV for TM = Co. Wang et al have also investigated the structural instability of the trigonal bipyramidal site for the M-type hexaferrite and demonstrate that that the ferroelectric state is energetically favourable with FE alignment of the dipoles along the c-axis and ferrielectric in the ab plane []. Importantly a compressive strain in the system of around 5% is shown to stabilize the ferroelectric state at room temperature. Although in Co-Ti doped hexaferrites not all the Fe cations in the 2b sites will be substituted by Co, the effect is clear. Increasing the occupation of Co into 2b sites enhances the ability for the structure to polarize as well as providing a magnetoelastic ion. Therefore, it seems that the Co substitution in the 2b sites provides a mechanism for an enhanced magnetoelectric effect.

5. SUMMARY AND CONCLUSIONS

In summary, we have used a combination of VSM magnetometry XAS / XMCD at the Fe and Co L_{2,3} edges to study the effect of Co substitution on the magnetoelectric coefficient in Co-Ti doped SrM hexaferrites. Multiplet features in the Co XMCD suggest that Co entering the trigonal 2b sites play an important role in the magnetoelectric effect in these materials. Naively one may expect α to

increase with the amount of Co in the octahedral sites due to the increased magnetoelasticity. However, it seems that the situation is more complex and that both magnetoelasticity and a mechanism for increasing the stability of the electric polarization are important for enhancing α . Doping into both the R and S block, with Co occupying the tetrahedral / trigonal sites and Ti occupying octahedral sites, are important for maximising the magneto-electric coupling.

Acknowledgements

The authors would like to acknowledge Professor M. J. Probert for fruitful discussions and to Diamond Light Source for the provision of beamtime under SI-10361, SI-12565 and SI-14135.

References

- [1] Y. Kitagawa, *et al.* Nature Materials **9**,797–802 (2010)
- [2] R.C. Pullar. Progress in Materials Science **57**, 1191 (2012)
- [3] J. Smit and H. P. J. Wijn. Ferrites. Philips Technical Library, (1959)
- [4] A Tauber, J. A. Koctahedraln and R. O. Savage. J Appl Phys 34, 1265 (1963)
- [5] M. Soda, *et.al.* Phys. Rev. Lett. **106**, 087201 (2011)
- [6] P. Borisov *et al.* Appl. Phys. Lett. **102**, 032902 (2013)
- [7] T. Kimura *et al.* Phys. Rev. Lett. **94**, 137201 (2005)
- [8] L. Wang *et al.* Sci. Rep **2**, 223 (2012)
- [9] M. Moctahedralebbi, K. Ebnabbasi, and C. Vittoria. J. Appl. Phys. **113**, 17C710 (2013)
- [10] H. Izadkhah, *et al.* Appl. Phys. Lett. **106**, 142905 (2015)
- [11] C. Vittoria, S. Somu and A. Widom, Phys. Rev. B **89**, 134413(2014)
- [12] G. F. Dionne, "Magnetic Oxides", Springer (2009)
- [13] R. Karim and C. Vittoria, JMMM 167, 27(1997); A. Geiler *et al.* Phys. Rev. Lett. **101**, 067201 (2008)
- [14] S. S. Dhesi, *et al.* AIP Conference Proceedings **1234**, 311 (2010)
- [15] S. Shen, Y. Chai and Y. Sun. Sci. Reports **5**, 8254 (2015)
- [16] G. van der Laan, Phys. Rev. B **34**, 6529 (1986)
- [17] Core level spectra were simulated using the CTM4XAS software (E. Stavitski and F.M.F. de Groot, Micron **41**, 687 (2010)) with the following parameters: 10Dq (Octahedral) = 1.9eV, 10Dq (Tetrahedral) = -0.9eV with Slater parameters reduced to 80% of the HF values. The Lorentzian broadening values used for each peak in the simulated spectrum were 0.1 eV, 0.6 eV, 0.5 eV, and 1.0 eV respectively.
- [18] D.J. Huang *et al.* Phys. Rev. Lett **93**, 077204 (2004)
- [19] The following parameters were used for the calculations. 10Dq (Octahedral) = 1.1eV, 10Dq (Tetrahedral) = -0.5eV with Slater parameters reduced to 72% of the HF values. For the trigonal bipyramidal sites the C3i symmetry was used with 10Dq = 0.8eV, D τ = -0.08eV and D σ = 0.01eV. We note for these values of the crystal field parameters the five d-orbitals break up into two doublets ${}^2E''(d_{zx}, d_{yz})$ and ${}^2E'(d_{x^2-y^2}, d_{xy})$ plus a singlet ${}^2A'_1(d_{z^2})$ with ${}^2A'_1 > {}^2E' > {}^2E''$ as expected for this symmetry.
- [20] J. Kreisel, *et al.* J. Magn. Magn. Mater. **224**, 17 (2001). X. Batlle, *et al.* J. Appl. Phys. **70**, 1614 (1991).
- [21] W. Eerenstein *et al.* Nature **442**, 759 (2006)
- [22] M. Javed Iqbal *et al.* Journal of Magnetism and Magnetic Materials **322**, 1720 (2010)
- [23] J. M. Williams *et al.* JMMM **220**, 124 (2000)
- [24]
- [25]
- [26]

Figure Captions

Figure 1: Perspective view of the M-type structure showing Wyckoff positions, co-ordination and block of the cations.

Figure 2: VSM magnetometry for $\delta = 0.0, 0.2$ and 0.4 . $M(T)$ for (a) $\delta = 0.0$, (b) $\delta = 0.2$ and (c) $\delta = 0.4$ measured at 300 Oe for FC and ZFC conditions. (c) $M(H)$ loops for $\delta = 0.0$ (red), $\delta = 0.2$ (blue) and $\delta = 0.4$ (green) measured at 300K.

Figure 3: Change in M as a function of applied voltage, V , for (a) $\delta = 0.0$, (b) $\delta = 0.2$ and (c) $\delta = 0.4$. Measurements were taken with an applied bias field of 400Oe with E parallel to M .

Figure 4: Ti $L_{2,3}$ XAS measured for $\delta = 0$ and $\delta = 0.2$ at 300K in TEY (red data points). The blue solid line is the simulated spectra from an atomic XAS multiplet calculation of Ti^{4+} in an octahedral co-ordination with $10Dq = 1.9$ eV. The black dashed line is an equivalent calculation for Ti^{4+} in a tetrahedral co-ordination with $10Dq = -0.9$ eV.

Figure 5: XAS and XMCD spectra for (a,c) $\delta = 0.0$ and (b,d) $\delta = 0.2$ at the Fe (upper) and Co (bottom) $L_{2,3}$ edges respectively. Spectra were measured at $T = 230K$, $\mu_0H = 6T$ and with the X-ray propagation vector parallel to H and at 60 degrees with respect to the surface normal. Fits to the data (green) using atomic multiplet calculations are shown in black.

Figure 6: The calculated energy potentials from Eq. (2) for $U_{repulsion}$ as a function of off-equatorial displacements (z) for (a) Fe^{3+} and (b) Co^{2+} in the trigonal bi-pyramidal site.

Figure 1

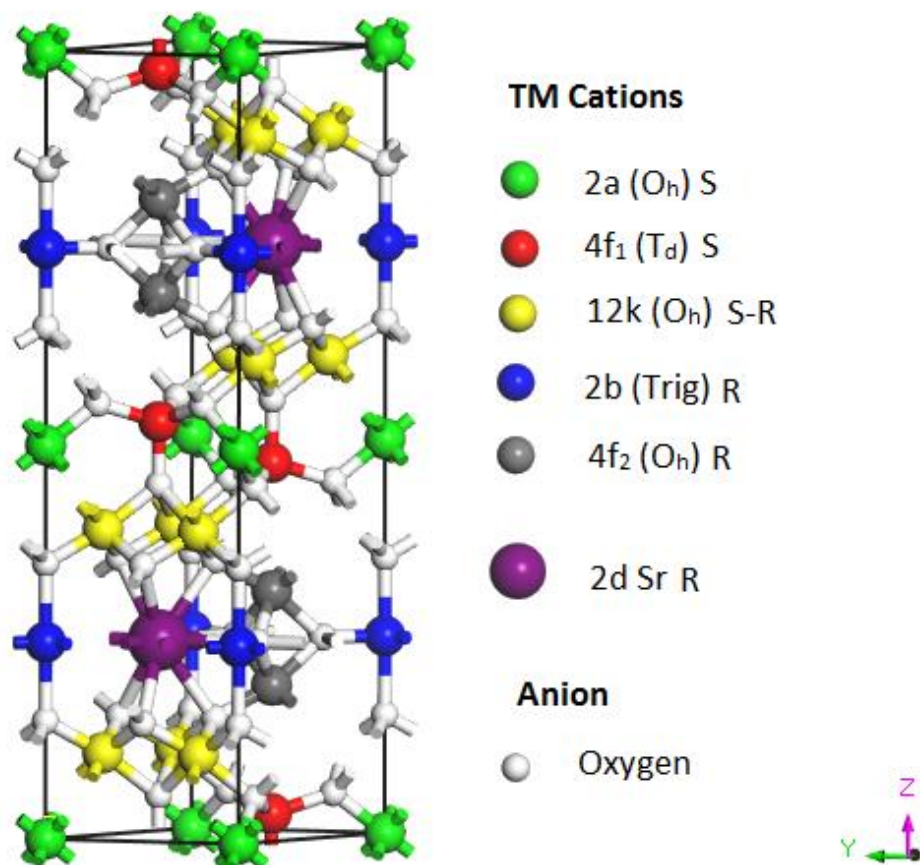


Figure 2

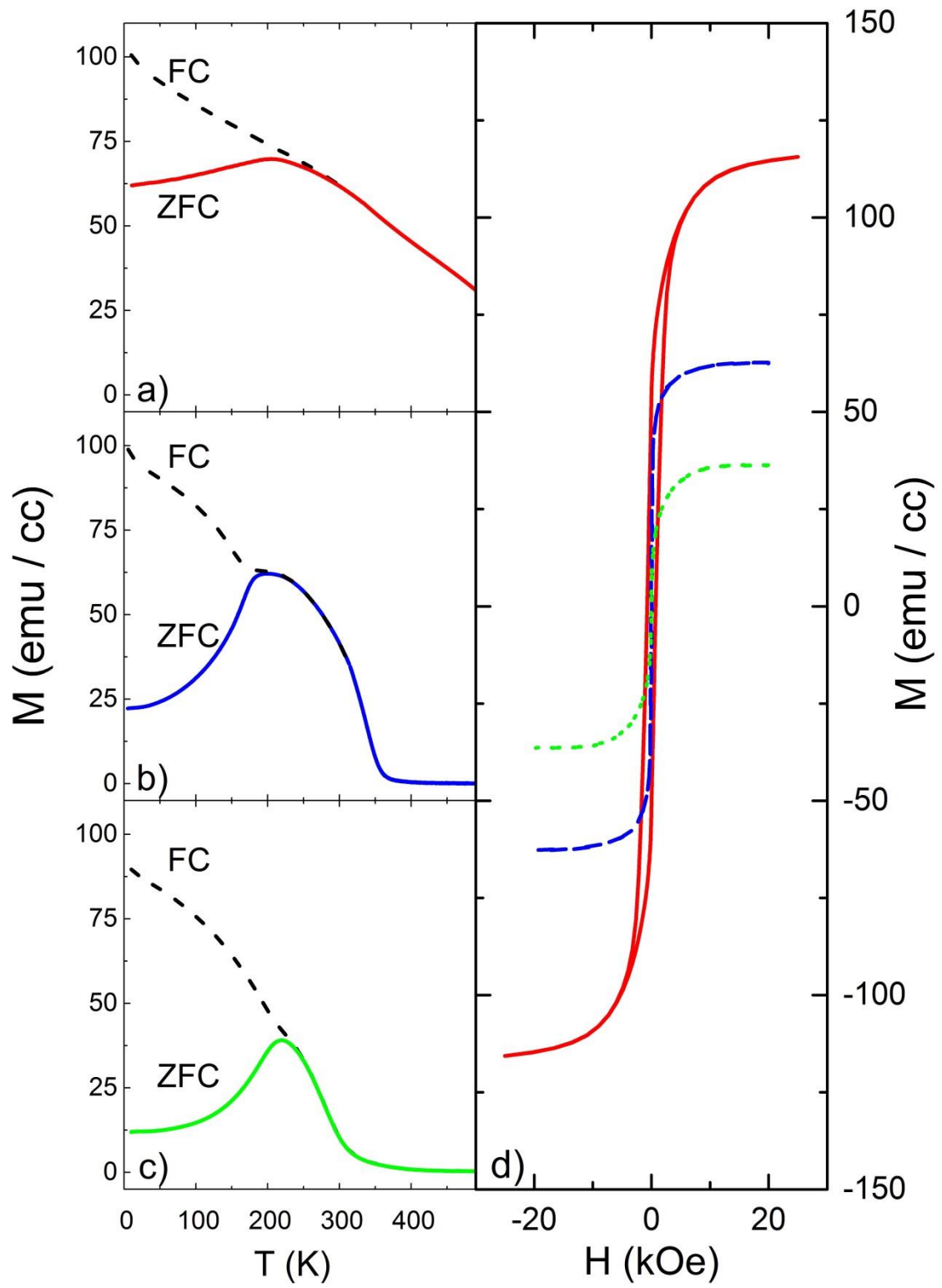


Figure 3

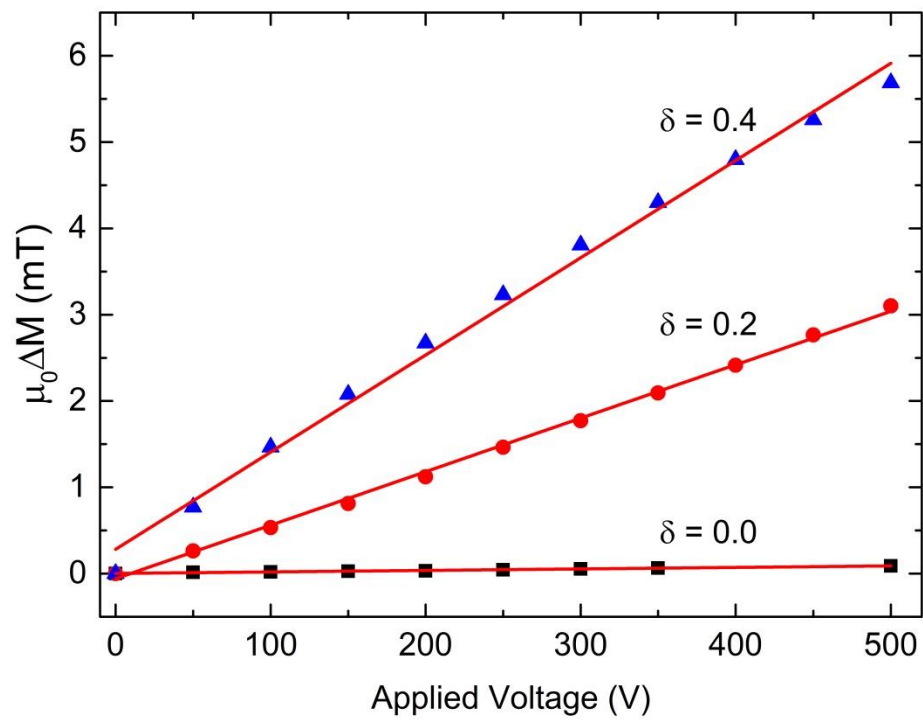


Figure 4

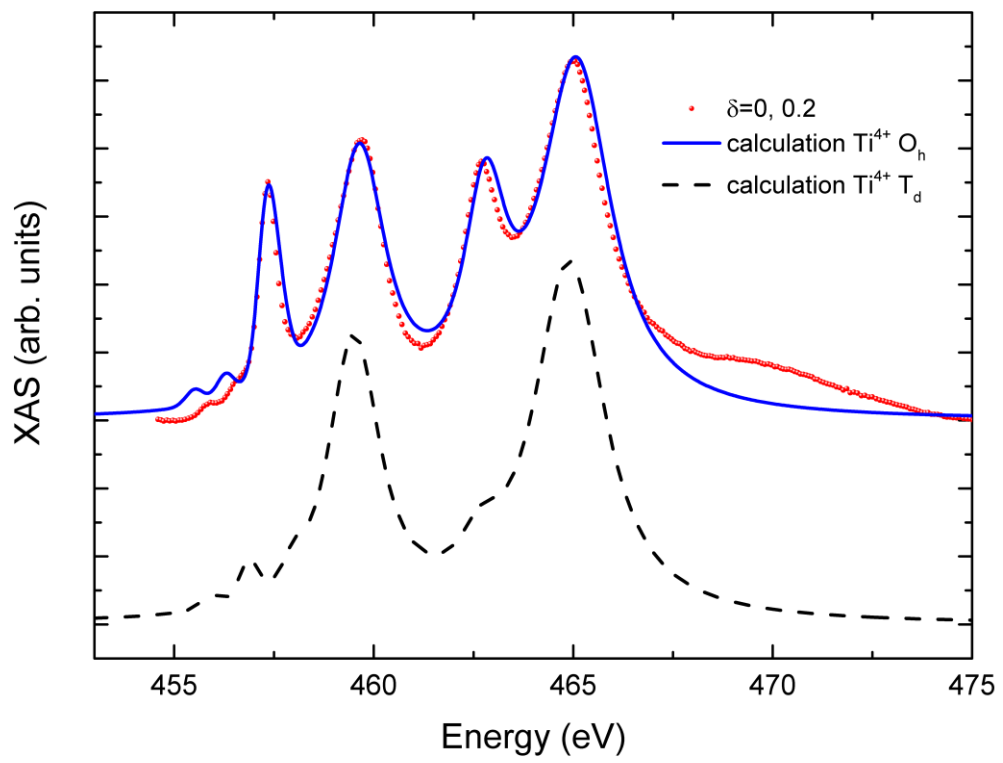


Figure 5

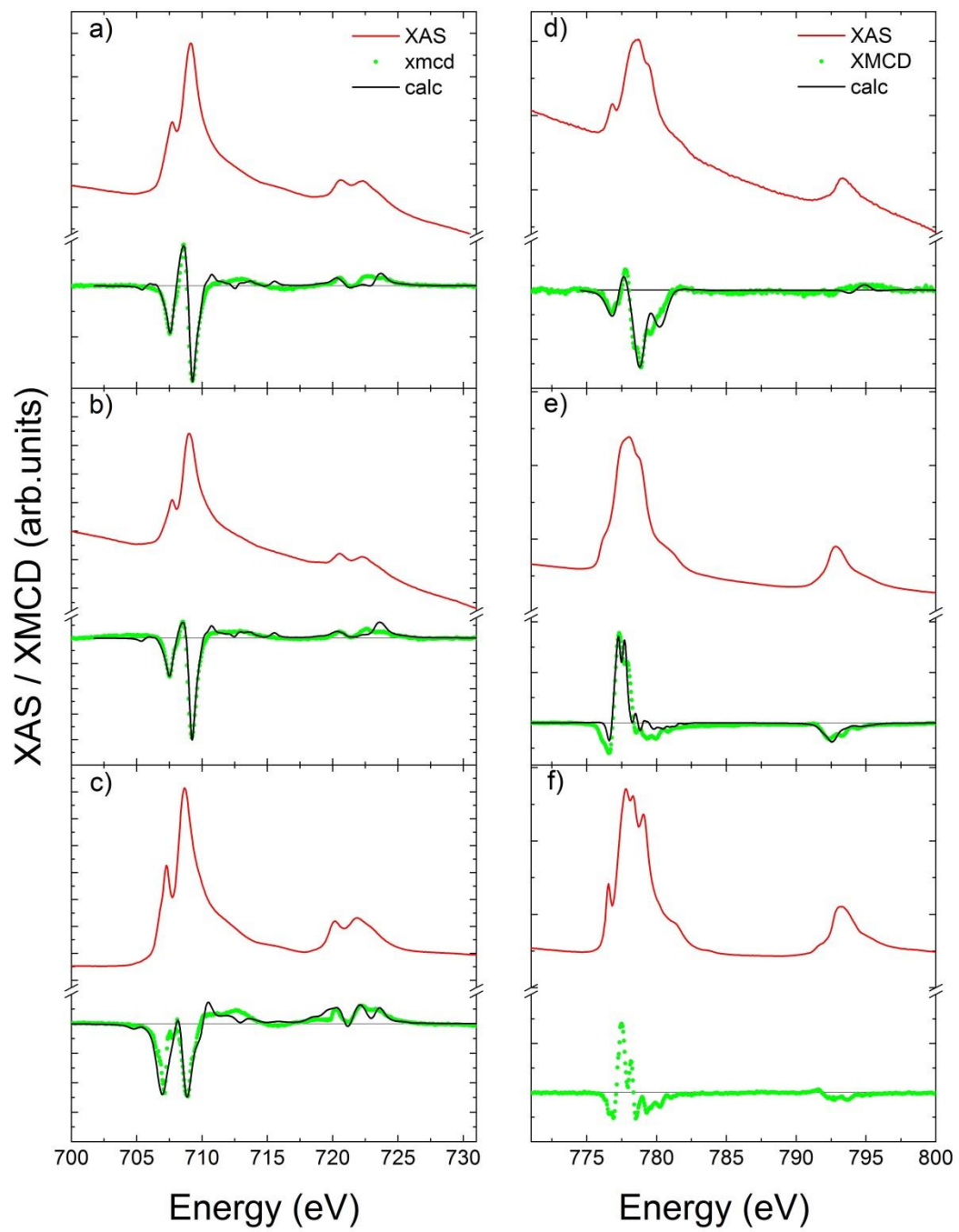


Figure 6.

